Vortex formation on squared and rounded tip

Michea Giuni[a,*], Richard B. Green[a]

[a]*Department of Aerospace Engineering, University of Glasgow, G12 8QQ, Scotland, UK*

Abstract

The vortical flow originated from the tip of a NACA 0012 rectangular wing is described in its initial formation and development over a rounded and a squared tip. Smoke visualizations show the rolling-up kinematic and evolution of the vortical systems moving the plane towards the trailing edge. The presence of intense secondary vortices affects the primary vortex unsteadiness and shape during the formation and in the early wake. Stereoscopic Particle Image Velocimetry is used to describe vorticity, axial velocity and turbulent kinetic energy distributions of the vortex during the formation and in the early wake at different angles of attack of the wing. The rolling-up of the vorticity sheet around the vortex system is strongly influenced by the vortex shape and the intensity of secondary vortices. Turbulence coming from secondary structures and shear layers is wrapped into the roll-up of the vortex and high levels of turbulence are measured in the vortex core. However, a laminar vortex core is observed for the lower angle of attack in the early wake. Comparing the meandering of the vortex for the two wingtip geometries, two different sources of the vortex fluctuation in the wake are identified: the interaction of secondary vortices moving around the primary vortex and the rolling-up of the vorticity sheet. Lastly, measurements in the wake of the wing at zero incidence are also presented showing a distinctive counter rotating vortex pair.

Keywords: Wingtip vortex, Smoke visualization, Stereoscopic Particle Image Velocimetry, Wingtip geometry, Vortex merging

1. Introduction

It is well known that the flow behind a lifting surface, such as a wing, results in a persistent and intense pair of organized vortical structure called trailing vortices or wingtip vortices. Whereas the evolution, the characteristics, the structure of these vortices have been extensively investigated, its origin is often misrepresented. Green [1] explains the occurrence of the tip vortices in three distinctive and complimentary ways. The first and commonly adopted considers the pressure difference between the wing pressure and suction surfaces which accelerates the fluid around the tip. This movement, combined with the streamwise velocity component, produces a vortical structure. A second and more schematic explanation involves Helmholtz vortex laws which present the tip vortices as the connections between the bound vortex (net circulation around the wing, from Kutta-Jukowski law) and the starting vortex (matching of wing circulation when the wing starts to move, from Kelvin's theorem). A third way to explain tip vortices is in terms of shear layer that exists near the tip. The undisturbed flow and the flow over the wing surfaces are not parallel which implies vorticity approaching the tips. This mechanism allows for two vortices of opposite sign behind each wingtip without producing lift. However, what is observed is that the trailing vortex is more complex than these mechanisms and the flow at the wingtip involves development and interactions of multiple vortical structures, shear layer instabilities, three-dimensional separations and reattachments; in the wake, rolling-up of the vorticity sheet, vortex instabilities, decay and diffusion, vortices interaction and merging are observed. Furthermore the formation and development is strongly affected by several factors such as wing geometry, tip geometry, wing load distribution, vortex circulation and nature of the boundary layer on the wing.

Moreover, many studies focused on the modification and control of the vortex through wingtip devices such as passive (static) methods based on changes in the wing configuration (vortex generators, winglets, wingtip mounted propellers, different tip geometries,

*Corresponding author.

Email address: michea.giuni@glasgow.ac.uk (Michea Giuni)

splines, spoilers) and active (dynamic) methods. In the latter devices, continuous or periodic controls are adopted such as blowing, active Gurney flaps, boundary layer separation control, active surface mount actuators. However, although many studies on wingtip vortices have been conducted, studies on the detailed flow physics are not that numerous. The complex three-dimensional flow near the tip is not adequately described, especially regarding the vortex unsteadiness and the mechanism of vorticity transport from the near-surface viscous layers into the concentrated trailing vortex.

Chow et al. [2] presented a study on the initial roll-up and early wake evolution of the tip vortex over a rounded wingtip. The secondary and tertiary vortices merges into the primary vortex within one chord from the trailing edge of the wing and the form an axial-symmetric vortical structure with axial velocity higher then the freestream (jet-like). As Freymuth et al. [3] stated, flow visualization seems to be the best approach to obtain clues about complex vortical structures and many studies on this phenomenon begins with flow visualizations [2, 4, 5]. Since the squared tip is a source of singularities in theoretical or numerical analysis, the study of flow over such geometry is particularly significant [6]. Bailey et al. [7] adopted different experimental techniques in order to investigate the evolution of the vortex on a squared tip. The wingtip vortex was found to be formed by three distinct co-rotating vortices. Smoke visualizations performed by Katz and Galdo [5] showed the complex multiple vortices structure and interaction. Secondary vortices are formed on the side of the wing and eventually they climb around the corner contributing to the unsteadiness of the primary vortex. PIV measurements on squared tip by Birch et al. [8] confirmed the multiple vortices structure in the initial rolling-up of the vortex and they showed both axial velocity deficit and excess in the vortex centre at a distance of 1.5 chords from the trailing edge. Karakus et al. [9] concluded that the tip region is dominated by the strong interaction between the multiple secondary vortices and the primary vortex. Zuhal and Gharib [10] found this interaction also in the wake up to 3 chords of distance from the wing; they also found a correlation between a higher fluctuation of the primary vortex location and the presence of strong secondary vortices.

The random movement of the vortex on the plane perpendicular to its axis is commonly known as meandering or wandering and it can be attributed to a variety of reasons including freestream turbulence, vortex instabilities, perturbation due to the rolling-up shear layer and unsteadiness originating on the model [11, 12]. Therefore, the understanding of mechanisms and effects of these contributes to the meandering is crucial in the correlation of different experiments and numerical analysis.

The meandering fluctuation is often identified and subtracted from instantaneous flowfields before the average flow is evaluated [e.g. 13, 14]. However, this operation does not completely eliminate turbulence in the vortex flow which sources can be found in the boundary layer, viscous wake (streamwise shear), vortex sheet (lateral shear), vortex circulation and atmosphere [15]. The turbulence distribution in the vortex flow and the evolution of the turbulence inside the vortex core has been a matter of many experimental and theoretical studies [e.g. 16, 17]. Phillips [18] described the relaminarization process and the resulting solid body rotation of the inner core as the result of high centrifugal forces which dissipate the turbulence at a rapid rate. Cotel and Breidenthal [19] presented a model for stratified entrainment so that turbulent diffusion is limited and the growth of the vortex is essentially dictated by molecular viscosity. Chow et al. [20] presented high turbulence level in and around the vortex core in the early wake coming from the wingtip boundary layers being wrapped during the roll-up of the vortex. They also linked the generation of turbulence with the high radial gradients of the axial velocity within the vortex core.

2. Experimental procedure

The wing model tested was a rectangular planform with NACA 0012 profile, 0.76 m chord and 0.75 aspect ratio. Squared and a rounded wingtips were tested. The wing area with the round cap was around 7% greater than the wing area with squared tip. The model was mounted vertically on a circular plate on the floor allowing the angle of attack to be adjusted by rotation about the quarter chord, coincident with the middle plane of the test section.

The reference systems adopted in these experiments are sketched in Fig. 1. A fixed reference system $x-y-z$ with origin at the trailing edge of the tip at angle of attack $\alpha = 0°$, with x directed as the freestream, was used. An additional coordinate $\tilde{x}$ with origin at the leading edge and directed as the wing chord c was also adopted for the experiments on the vortex formation on the wing.

Two experimental techniques were adopted and two wind tunnels were used for the experiments: a low speed open circuit wind tunnel for smoke visualizations on the initial roll-up and formation of the vortex on the wing; a subsonic return wind tunnel for Stereoscopic

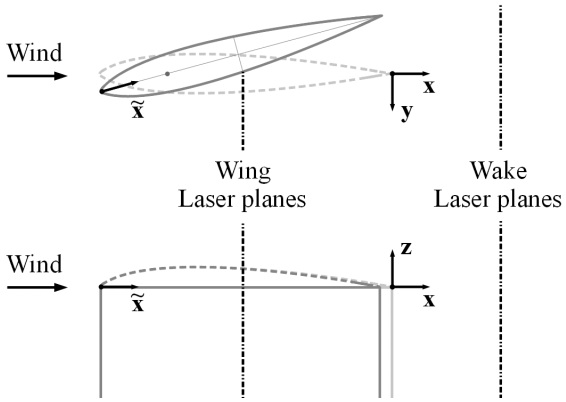

Figure 1: Experimental arrangement.

Particle Image Velocimetry on vortex formation on the model and development in the wake.

2.1. Smoke visualization technique

Smoke visualizations were conducted in a purpose built flow visualization wind tunnel with cross section of 0.91 m by 0.91 m. The two tip geometries were tested at a Reynolds number of 3,000 at 12° of angle of attack. The smoke lines were illuminated with a continuous laser sheet of 2 mm thickness from a diode laser (5 W power at 532 nm) which was shone from the top of the test section and perpendicular to the freestream flow. A high resolution camera (DALSA 2M30) of 1600 by 1200 pixels with 50 mm focal length lens and f-number equal to 4 was mounted 1.5 chords downstream of the trailing edge of the wing and it was used to capture the initial roll-up and the wingtip vortex formation at several locations along the chord. The exposure time was set in a range between 1 and 400 ms so that the vortex system was clearly visible.

The smoke tracer was Shell Ondina EL oil and high pressure carbon dioxide was used as a propellant. The smoke was injected through uniformly distributed orifices of 1 mm of diameter and 6.35 mm step, drilled on a pipe of 12 mm of diameter positioned vertically in the centre of the test section inlet (1 chord upstream of the leading edge of the wing). Pressure, density and velocity of the smoke at the orifices were set so that smoke filaments did not show disturbances.

2.2. Stereoscopic Particle Image Velocimetry

The SPIV experiments were conducted in a low-speed, closed-return facility with test section dimensions of 2.65 m wide by 2.04 m high by 5.60 m long and turbulence level of 0.4%.

Two CCD cameras of 11 Mpixels were mounted on one side of the test section independently from the wind tunnel and 200 mm focal length Nikon lenses were used with f-number equal to 8. The angular stereoscopic system in Scheimpflug condition was adopted, as described by Zang and Prasad [21]; the angles between cameras and object plane were between 40° and 47°. These values maintain low errors in the evaluation of both the in-plane and out-of-plane velocity components [22]. A double-frame/single-pulse method [23] was used so that at each time step two images were recorded by each camera in correspondence with two different laser pulses. The time delay used was calculated following the method described by Giuni et al. [24] assuming the maximum wind speed of the same order of the freestream velocity which leads to a notional displacement for the scaling velocity of 10 pixels. The light source of the laser sheet was provided by a dual cavity Nd:YAG laser with 532 nm wavelength. A laser guiding arm was installed on a rail placed above the test section which allowed two-dimensional translations and three axes rotations. The laser sheet, of 3 mm of thickness, was shone in the test section through a window on the top by a divergent lens. Glare problems are common when laser is used and they can limit the accuracy of the results in the vicinity of objects. In order to avoid glare off the model surface for the measurements on the vortex formation on the wing, the triangular laser sheet was rotated so that one edge was parallel to the wing surface and at a distance from it of about 8 mm. Every time the laser sheet was moved, the cameras were re-adjusted (angles and separation) and a new calibration was performed using a dual-plane calibration plate with circular markers aligned with the laser sheet. A LaVision PIV system with DaVis v7.2 software was used for calibration, image acquisition, laser control and stereo cross-correlation. Multiple images of the calibration grid at small, arbitrary rotations were taken according to the PIV system instruction manual [25]. Correlation coefficients calculated by the calibration scheme were satisfactory and within the system manufacturers guidelines. The stereo cross-correlation of the image pairs was a double step process on an interrogation window of 64 by 64 pixels with 25% of overlap followed by other two steps with interrogation window of 32 by 32 pixels with 50% of overlap leading to the calculation of around 50000 vectors per frame with spatial resolution between 0.18 and 0.23 percent of the chord, depending on the streamwise location of the laser sheet.

The flow was seeded through a pipe mounted downstream the test section with olive oil particles generated by a Laskin nozzle aerosol generator. The nominal peak

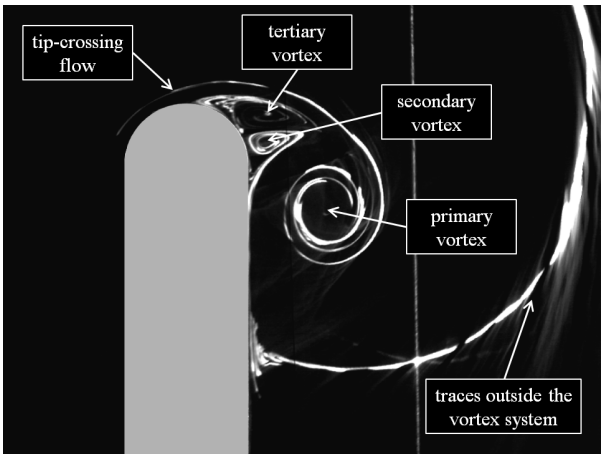

Figure 2: Vortex at $Re = 3000$, $\tilde{x}/c = 0.75$ and $\alpha = 12^\circ$ on rounded tip; wing section in gray.

in the probability density function of the olive oil particles size was at 1 μm that corresponds, following the procedure described by Adrian [26], to a particle diameter between 1 and 2 pixels which is what Prasad et al. [27] suggest to ensure a good quality in the images correlation. The peak-locking effect in the velocity maps was calculated by DaVis 7.2 and it was observed to be well within the acceptable range [25] for both the in-plane and the out-of-plane components of the velocity vector.

The performance of the stereo PIV was benchmarked by taking measurements of a uniform flow, for which there were no significant velocity gradients across the field of view. Absolute accuracy of the SPIV measurements and the averaging process was evaluated to be better than 3 percent, which is adequate for a quantitative and comparative analysis of flowfields.

The wing was tested at a Reynolds number of 740,000 and angles of attack of 0°, 4° and 12°. Planes perpendicular to the freestream at $\tilde{x}/c = 0.5$, 0.75 and $x/c = 0.25$, 1 were investigated. Each test consisted in the acquisition of 121 images pairs at a constant frequency of 2 Hz. The scaling parameter for the velocities was the freestream velocity and for the turbulent kinetic energy (TKE) was the square of the freestream. The vorticity was calculated from the non-dimensional velocity field adopting an 8 points circulation method as described by Raffel et al. [28].

3. Results and discussion

3.1. Smoke visualization: vortex formation process

The smoke visualizations of the vortex over a rounded and a squared tip are presented at different planes perpendicular to the freestream ($y-z$ plane). The pictures refer to the wing at an angle of attack of 12° and Reynolds number of 3,000. The length scale of all theses images are the same and the wing section on the pictures was added during the post-processing.

A typical smoke visualization of a wingtip vortex system on a rounded tip is shown on Fig. 2. The dominant flow is perpendicular to the laser sheet and it generates discontinuous smoke lines which are more evident where the ratio between the cross-plane velocity and the in-plane velocity is high. The thick smoke lines coming from the top edge of the pictures are traces of the curved smoke filaments that have left the smoke pipe upstream the wing. If the smoke filaments did not bend, they would appear as discrete dots on the laser plane. The primary vortex is fed by the tip-crossing flow which moves from the pressure surface (left) to the suction surface (right) and forms a spiral around the primary vortex centre. A counter-rotating secondary vortex is formed at the foot of the primary vortex and a tertiary vortex is also observed between the secondary vortex and the tip-crossing flow.

With reference to the vortex evolution on the rounded tip presented on Fig. 3, the tip-crossing flow from the wing pressure surface is clear already at $\tilde{x}/c = 0.30$. The adverse pressure gradient is not strong enough and the radius not small enough to induce the separation of the flow from the surface and a circulating flow is not observed. However, a thickening of the boundary layer can be inferred. Numerical experiments on a rounded tip at similar conditions were performed by Duraisamy [29] who confirmed the presence of not separated crossing flow at an early stage of the vortex formation. The vortex system is remarkably different at $\tilde{x}/c = 0.40$ and

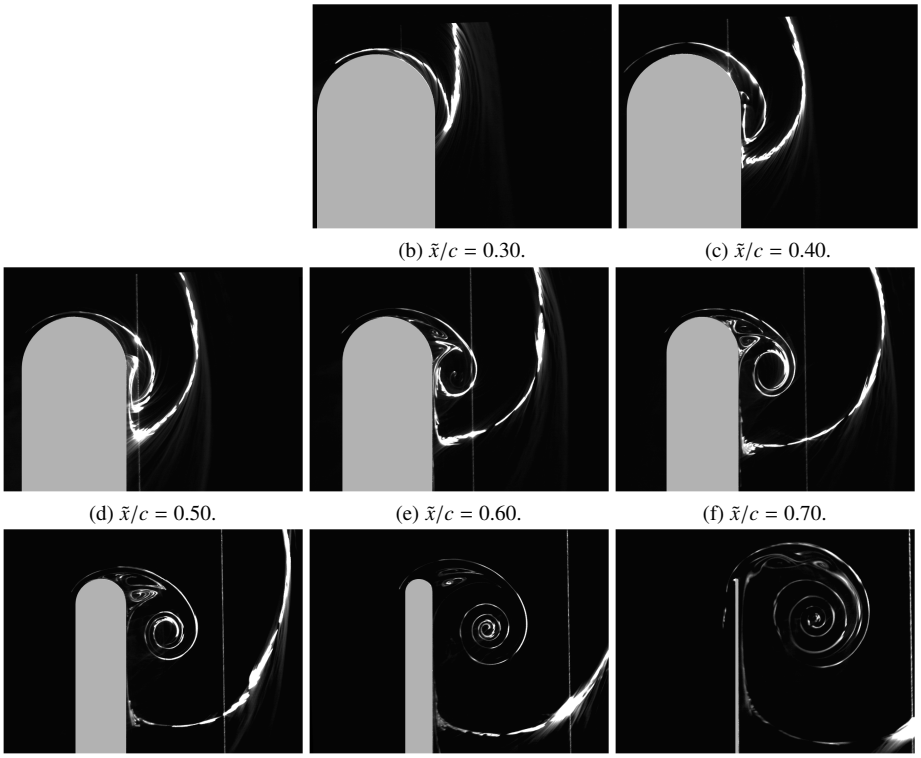

(b) $\tilde{x}/c = 0.30$. (c) $\tilde{x}/c = 0.40$.

(d) $\tilde{x}/c = 0.50$. (e) $\tilde{x}/c = 0.60$. (f) $\tilde{x}/c = 0.70$.

(g) $\tilde{x}/c = 0.80$. (h) $\tilde{x}/c = 0.90$. (i) $\tilde{x}/c = 0.99$.

Figure 3: Vortex evolution at $Re = 3000$ and $\alpha = 12^\circ$ on rounded tip; wing section in gray.

0.50, where the separation of the crossing flow generates a clear vortical structure which is squeezed on the surface. It was observed that the location of the plane where the vortex first appears is strongly affected by freestream conditions which generates an oscillating starting point. A similar vortex structure over a rounded tip was observed also by Chow et al. [2] at $\tilde{x}/c = 0.61$ for a Reynolds number of 4,600,000. At $\tilde{x}/c = 0.60$, the tip vortex system is made up of three vortical structures. Along with the primary vortex, a counter-rotating second vortex and a third vortex are formed. This vortex system is clearly seen at $\tilde{x}/c = 0.80$ where the secondary and tertiary vortices are enclosed between a bigger round primary vortex and the plane streamlines of the separated flow from the pressure side of the wing. At $\tilde{x}/c = 0.90$, the reduction in the thickness of the wing and the enlargement of the primary vortex pushes the secondary and tertiary vortices outboard. Finally, at $\tilde{x}/c = 0.99$, the secondary and tertiary vortices are not bounded by the surface anymore but they wrap around the primary vortex with the flow coming from the pressure surface.

At this Reynolds number of 3000, the tip vortex system on rounded tip is weakly time-dependent and the primary, secondary and tertiary vortices are well identifiable. At a fixed plane they do not move around but they form a stable multi-vortex system. At these conditions, the spiral shape from the rolling-up of the pressure surface is very clear.

On squared tip, the separation of the cross flow from the pressure surface to the suction surface does not happen smoothly but it is forced by the sharp edges of the wingtip. Therefore the number of vortices due to the separation increases and their interaction generates a time-dependent vortex system which enhances the mixing of the spiral layers. In the flow visualizations, a higher diffusion of smoke in the core of a vortex generated by a squared tip is then expected compared to the rounded tip case at the trailing edge.

The evolution of the tip vortex system over a squared tip is presented in Fig. 4. At $\tilde{x}/c = 0.20$, four vortices can be already identified. A first set of three vortices formed by the pressure surface-tip sharp edge (top surfaces of Fig. 4) appears in a similar form of the vortex system on rounded tip on Fig. 2. Another set of vortices is formed from the suction surface-tip sharp edge

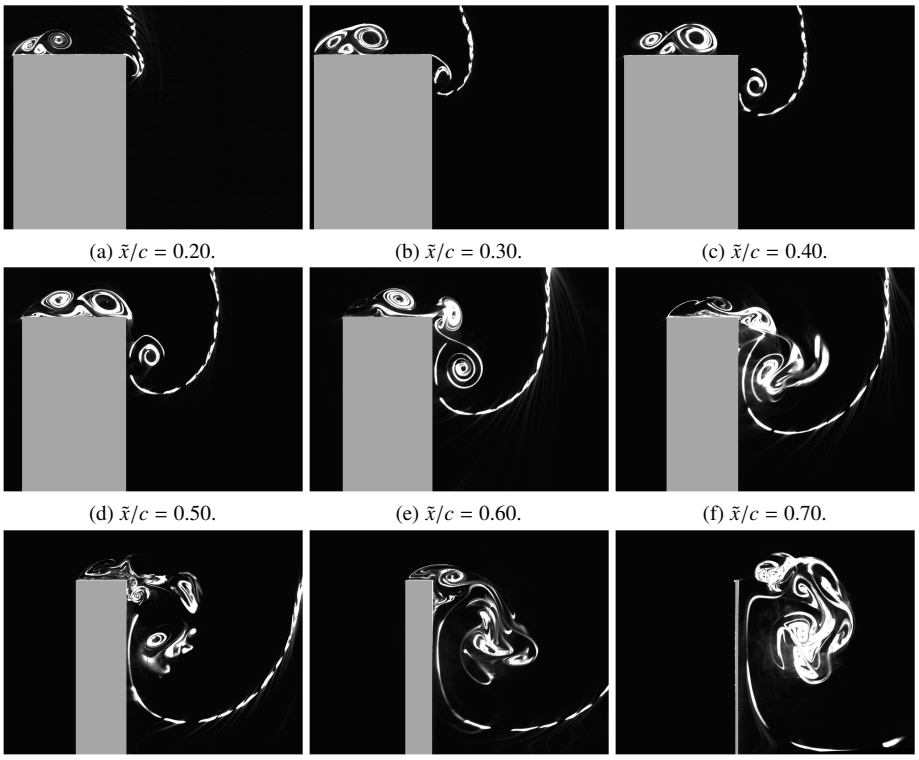

(a) $\tilde{x}/c = 0.20$. (b) $\tilde{x}/c = 0.30$. (c) $\tilde{x}/c = 0.40$.

(d) $\tilde{x}/c = 0.50$. (e) $\tilde{x}/c = 0.60$. (f) $\tilde{x}/c = 0.70$.

(g) $\tilde{x}/c = 0.80$. (h) $\tilde{x}/c = 0.90$. (i) $\tilde{x}/c = 0.99$.

Figure 4: Vortex evolution at $Re = 3000$ and $\alpha = 12^\circ$ on squared tip; wing section in gray.

(surfaces on the right side of Fig. 4) which encloses the vortical structure that will become the primary vortex. Initially the two sets seem to evolve independently of each other and no sign of strong time-dependency is observed. From $\tilde{x}/c = 0.20$ to $\tilde{x}/c = 0.50$ the vortices grow and the first vortex system moves towards the suction surface-tip edge stretching over the whole tip area. Similarly, Francis and Kennedy [6] investigated the flowfield around a squared tip of a rectangular wing with NACA 64009 aerofoil at a Reynolds number of 385,000. At an angle of attack of 4°, they did not observe regions of reverse crossflow on the suction surface for $\tilde{x}/c < 0.60$. However, a region of increasing size of reverse flow on the tip side was shown. At $\tilde{x}/c = 0.60$ the two vortex systems start to interact. The vortices from the first system move to the suction surface and they interact with the primary vortex modifying its shape and increasing the mixing of the spiral layers. At a fixed plane, these vortices fluctuate from the tip surface to the suction surface generating high level of unsteadiness on the primary vortex. In Fig. 10, a collection of snapshots is reported in order to highlight the unsteadiness when the two vortex systems interact; position, size and shape of secondary vortices are observed to vary rapidly. From $\tilde{x}/c = 0.70$, the primary vortex is wrapped by vortices coming from the tip which mix with the spiral layers. Several vortices, wrapping around the primary vortex, can be counted at $\tilde{x}/c = 0.80$ and $\tilde{x}/c = 0.90$. At this stage, the spiral layers are lost and the shape is dominated by the interaction with secondary vortical structures. At $\tilde{x}/c = 0.99$, the tip vortex is shed from the wing as a strongly unsteady vortex system which includes several secondary vortices.

It is believed that the kinematic of the tip vortex formation for these two geometries remains the same for a wide range of Reynolds number. Dye visualizations in a water tank have been presented by Francis and Katz [30] for a hydrofoil with squared tip at Reynolds number in a range between about 30,000 and 1,400,000. They observed similar multiple vortex structures and interactions in their cases. Moreover, they attributed the formation of secondary vortices as the flow separates at the pressure surface-tip edge close to the trailing edge to shear layer eddies.

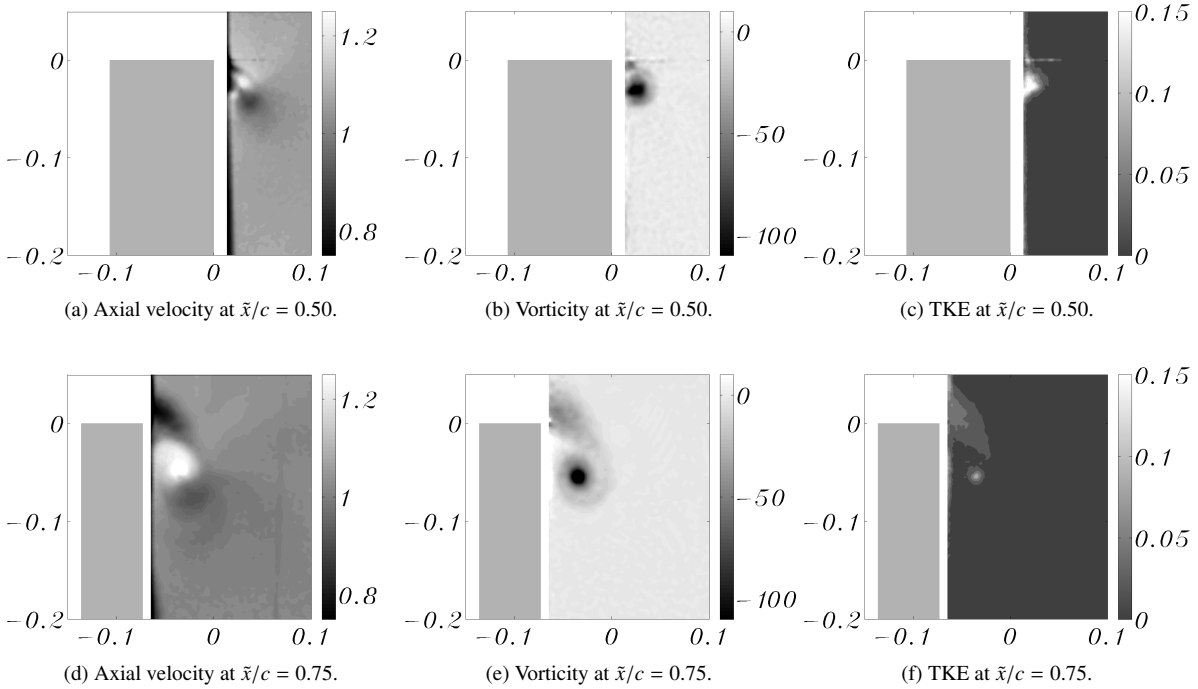

(a) Axial velocity at $\tilde{x}/c = 0.50$. (b) Vorticity at $\tilde{x}/c = 0.50$. (c) TKE at $\tilde{x}/c = 0.50$.

(d) Axial velocity at $\tilde{x}/c = 0.75$. (e) Vorticity at $\tilde{x}/c = 0.75$. (f) TKE at $\tilde{x}/c = 0.75$.

Figure 5: Squared tip at $\alpha = 12°$ and $Re = 740,000$; wing section in gray.

3.2. SPIV: vortex formation and near wake

SPIV measurements on planes perpendicular to the freestream were performed for the two tip geometries at angles of attack of 0°, 4° and 12°. The laser sheet was positioned for the measurements on the wing at $\tilde{x}/c = 0.5 - 0.75$ and in the wake at $x/c = 0.25 - 1$. The Reynolds number was 740,000. The averaged vector fields are reported on $y - z$ planes which are scaled by the chord. Non-dimensional axial velocity (velocity component parallel to the freestream), planar vorticity (vorticity component parallel to the freestream) and turbulent kinetic energy are presented.

Even though a widely accepted definition of a vortex has not been found yet, in particular regarding the study of coherent structures in turbulent flows [31, 32, 33, 34], wingtip vortices present a structure which is well identifiable. Rotation of a large portion of fluid around a common centre and a region of high vorticity within the vortex core (hence net circulation) are major elements of trailing vortices. Many studies have dealt with the centering of instantaneous planar measurements of a vortex, in particular when taking into account of the meandering. Ramasamy et al. [14] showed in detail how different aperiodicity correction methods applied on each vector field measured by a SPIV before the average is taken affect the description of a rotor tip vortex. The helicity peak correction method was seen to perform better than the vorticity peak, axial velocity peak, Q-criterion and zero in-plane velocity in the estimation of the swirl velocity peak, axial velocity peak and vortex core radius. Giuni and Benard [35] pointed out that the particular feature of the vortex which is studied also determines the choice of the centering method. This is especially true in the very near field where the vortex does not show a developed axisymmetric structure. Because the focus of the current study is on the rolling-up of the wake and in particular of the vorticity sheet shed by the trailing edge, no centering method was applied on the current measurements.

In Fig. 5, contours of axial velocity, vorticity and turbulent kinetic energy are shown on planes at $\tilde{x}/c = 0.5$ and $\tilde{x}/c = 0.75$ for the squared tip at $\alpha = 12°$ where the left side of the figure is the region not illuminated by the laser. The axial velocity (Figs. 5a and 5d) presents a pocket of jet-like fluid in correspondence of the centre of the vortex on both the planes. Regions of wake-like fluid come from the tip region and roll around the primary vortex. Lee and Pereira [36] observed a similar flowfield and they concluded that a region of jet-like fluid is always formed in the centre of the vortex.

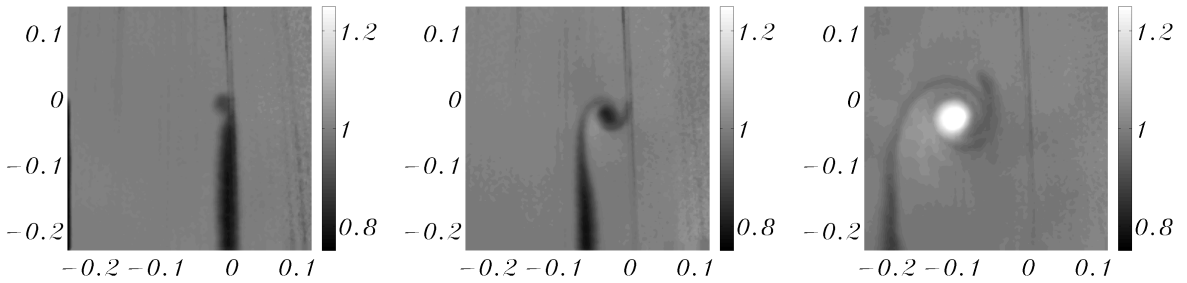

(a) Rounded tip at $\alpha = 0°$. (b) Rounded tip at $\alpha = 4°$. (c) Rounded tip at $\alpha = 12°$.

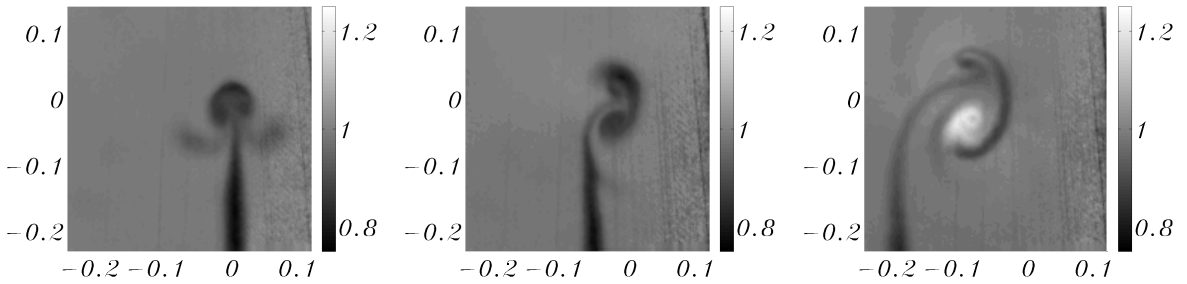

(d) Squared tip at $\alpha = 0°$. (e) Squared tip at $\alpha = 4°$. (f) Squared tip at $\alpha = 12°$.

Figure 6: Axial velocity at $x/c = 0.25$ and $Re = 740,000$.

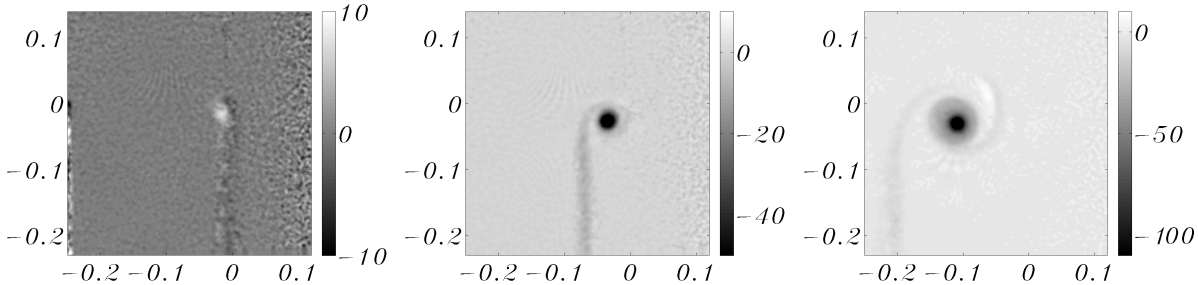

(a) Rounded tip at $\alpha = 0°$. (b) Rounded tip at $\alpha = 4°$. (c) Rounded tip at $\alpha = 12°$.

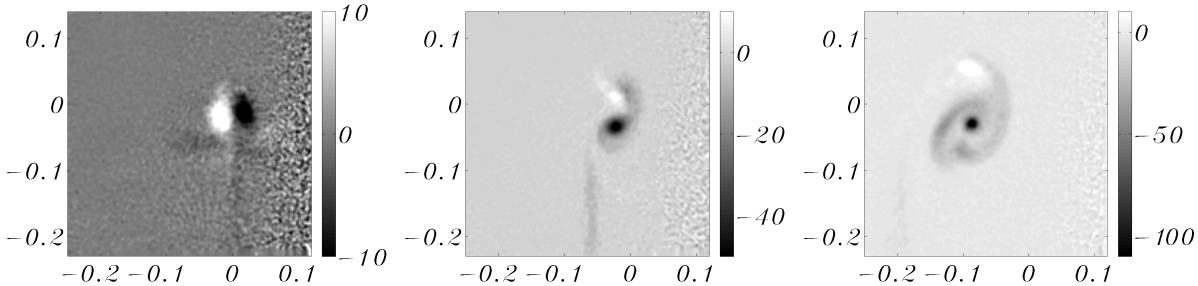

(d) Squared tip at $\alpha = 0°$. (e) Squared tip at $\alpha = 4°$. (f) Squared tip at $\alpha = 12°$.

Figure 7: Vorticity at $x/c = 0.25$ and $Re = 740,000$.

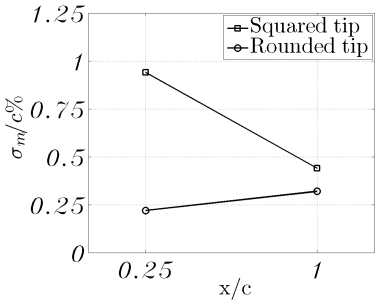

Figure 8: Vortex meandering at $\alpha = 12^\circ$ and $Re = 740,000$.

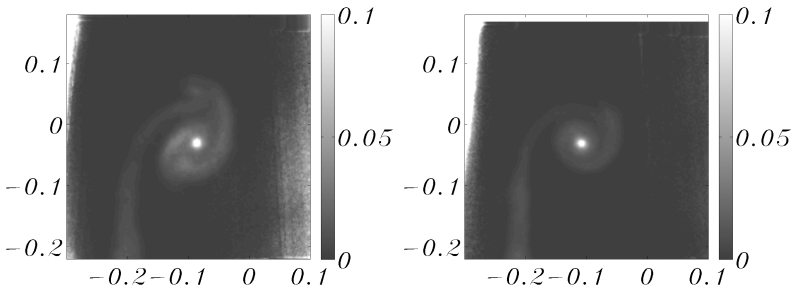

(a) Squared tip. (b) Rounded tip.

Figure 9: TKE in the wake at $x/c = 0.25$, $\alpha = 12^\circ$ and $Re = 740,000$.

They described this process as strongly dominated by the interaction of the vortex with the wing and the surrounding flow and therefore as function of several of parameters (i.e. tip geometry, multiple vortex structure, wing span, angle of attack, circulation and boundary layer properties). The jet-like flow region is then entrained by the shear layer and the wing wake during its formation and, depending on the tip vortex system intensity and structure, may develop into a wake-like flow as it progresses downstream. In the vorticity contours of Figs. 5b and 5e, the primary vortex shape can be clearly observed where a negative peak identifies its core. The rolling-up of the flow coming from the pressure surface can also be seen and another region of negative vorticity is detected in correspondence to secondary vortices from the tip where a wake-like fluid is recorded. On Figs. 5c and 5f, a high turbulence level region is observed in the vortex core. High turbulence is also observed for the flow from the tip region.

The axial velocity and the plane vorticity in the early wake of the wing with squared and rounded tip are reported respectively on Fig. 6 and on Fig. 7. At an incidence, the rolling-up of the vorticity sheet shed by the trailing edge of the wing, characterized by a low axial velocity, is observed. From a rounded tip, the vortex shows a more organized structure (i.e. axisymmetric) and a larger vorticity at the centre compared to the vortex formed by the wing with squared tip. The shape of the vortex from the squared tip is dominated by the interaction of the primary vortex with the numerous secondary vortices. A region of mean positive vorticity is located above the primary vortex and indicates the main counter rotating secondary vortex. The shape of the rolling-up vorticity sheet is strongly affected by the presence of this secondary vortex, as observed in the axial velocity contours. For an incidence of 12°, the vortex centre presents an axial velocity excess, higher for the rounded tip, surrounded by a region of axial velocity defect which is related to the vorticity sheet, as described by Giuni et al. [37].

Instantaneous vorticity fields of the vortex system generated by a wing with squared tip are presented in Fig. 11. A chaotic and intense interaction between primary vortex, vorticity sheet and secondary vortices is observed. The primary vortex position and shape change over the time induced by the main secondary vortex (counter-rotating structure above the primary vortex), other secondary vortices and the rolling-up vorticity sheet. The vortex meandering is evaluated by calculating the fluctuation of the primary vortex centre defined as the location of the streamwise helicity peak. The meandering of the vortex at different positions in the wake behind squared and rounded tips is reported on Fig. 8 as percentage of the chord length. The meandering of the vortex behind a squared tip is higher than the meandering behind a rounded tip. However, opposite trends of the meandering moving downstream in the wake are observed. The meandering behind the squared tip decreases with the distance from the trailing edge suggesting that the main source of the wandering in the very early wake come from the interaction of the intense secondary vortices, as observed also by Zuhal and Gharib [10], which dissipate and are then absorbed by the primary vortex. Conversely, the meandering from a wing with rounded tip in the early wake is dominated by the essentially inviscid smoothing out process of the spiral vorticity sheet and it grows almost linearly with the distance as observed by Devenport et al. [13].

In the formation of the vortex on the wing, turbulence coming from the tip-crossing flow is entrained during the roll-up. Consequently, the vortex core in the very early wake at $x/c = 0.25$ is turbulent for both the geometries as observed in Fig. 9 for $\alpha = 12^\circ$. The turbulence of the wake sheet can also be observed as a verti-

cal turbulent region. The turbulence peak is located at the centre of the vortex and similar values are found for the two tip geometries. For $\alpha = 4°$, almost zero turbulence was measured in the whole velocity field which indicates an already relaminarized flow. Jiang et al. [38] found that the turbulent shear layer and the interaction between the primary and the secondary vortices are major sources of the turbulent activity in the core which are more intense for the higher angle of attack. As the vortex for $\alpha = 12°$ moves downstream and develops into an axisymmetric flow, a relaminarization of the vortex core and a consequent lowering of the turbulence is then expected. Devenport et al. [13] reported fluctuations in the vortex core in a range between 5 and 30 chords from the wing and they attributed these fluctuations to inactive motions produced by turbulence from the surrounding wake or by wandering and not by turbulence in the vortex core which was laminar.

At zero angle of incidence (thus no lift), the squared tip generates a symmetric wake formed by two opposite vortices of the same order of the secondary vortex for the wing at an incidence (Figs. 6d and 7d). This phenomenon is described by Green [1] as the consequence of the non-parallelism of the vectors of the freestream velocity and the flow over the wing surface which implies two vorticity sources of opposite sign and same magnitude. The two vortices are formed on the two wing surfaces and they are fed by the flow on the tip side forced to a separation by the sharp edges. At $x/c = 0.25$, the vortex pair does not show a remarkable asymmetry. For the rounded tip (Figs. 6a and 7a), the wake shows a smaller and weaker vortex pair at the edge of the vorticity sheet. The importance of this phenomenon in the initial formation of the wingtip vortex is underestimated and only few mentions can be found in the literature. Although the tip geometries tested in this work are very simple, they highlight the complexity and basics of this fundamental mechanism of vortex formation providing an important benchmark for numerical analysis on the flow around wingtips.

4. Conclusions

The study of the formation and early wake of a wingtip vortex formed over squared and rounded wingtips has revealed two different causes of the vortex meandering depending on the wingtip geometry. Squared tips present two sharp edges and produce a multiple vortex structure with highly unsteady secondary vortices. These vortices highly contribute to disturb the primary vortex generating more unsteadiness on the model and in the early wake. The unsteadiness of the primary vortex due to the interaction with secondary vortices is the main source of the meandering and it decreases with the distance from the trailing edge as the secondary vortices dissipate. A vortex formed by a wing with rounded tip presents fewer and less intense secondary vortices than one from a squared tip and it reaches axisymmetric flow condition at an earlier stage. However, the main source in the meandering for this geometry is related to the vorticity sheet which rolls-up around the vortex as it moves downstream, so that the fluctuations increase with the distance from the trailing edge. The importance of relating the vortex formation, and so the wingtip geometry, with the unsteadiness in the wake is one of the key steps of vortex control devices.

During the formation of the vortex on the wing, turbulence coming from the tip-crossing flow is entrained in the vortex core resulting in a turbulent core in the early wake. For low vortex intensity, hence small radial gradients of the axial flow, the relaminarization process rapidly dissipates the turbulence in the core downstream of the trailing edge. The turbulence production during this process is directly linked to the radial gradient of the axial flow, as found by Chow et al. [20]. The direction of the axial flow and its intensity, jet-like or wake-like, plays therefore a crucial role in the early evolution of the wingtip vortex.

An important mechanism in the wingtip vortex formation is highlighted at zero incidence of a wing with a symmetric profile where a counter-rotating vortex pair is generated. The numerical simulation of this vortex system, which is more intense and distinct for the squared tip, is suggested as benchmark for numerical codes aiming to describe the flow physics of the formation and early wake of wingtip vortices.

Acknowledgements

This research was supported by the Scottish Funding Council.

References

[1] S. I. Green, Fluid vortices, in: Fluid Mechanics and its Applications, Kluwer Academic Publisher, 427–470, 1995.

[2] J. S. Chow, G. G. Zilliac, P. Bradshaw, Initial Roll-Up of a Wingtip Vortex, in: Proceedings of the aircraft wake vortices conference, vol. 2, Federal Aviation Administration, 1992.

[3] P. Freymuth, F. Finaish, W. Bank, Visualization of wing tip vortices in accelerating and steady flow, Journal of Aircraft 23 (9) (1986) 730–733.

[4] M. H. Sohn, J. W. Chang, Visualization and PIV study of wingtip vortices for three different tip configurations, Aerospace Science and Technology in press.

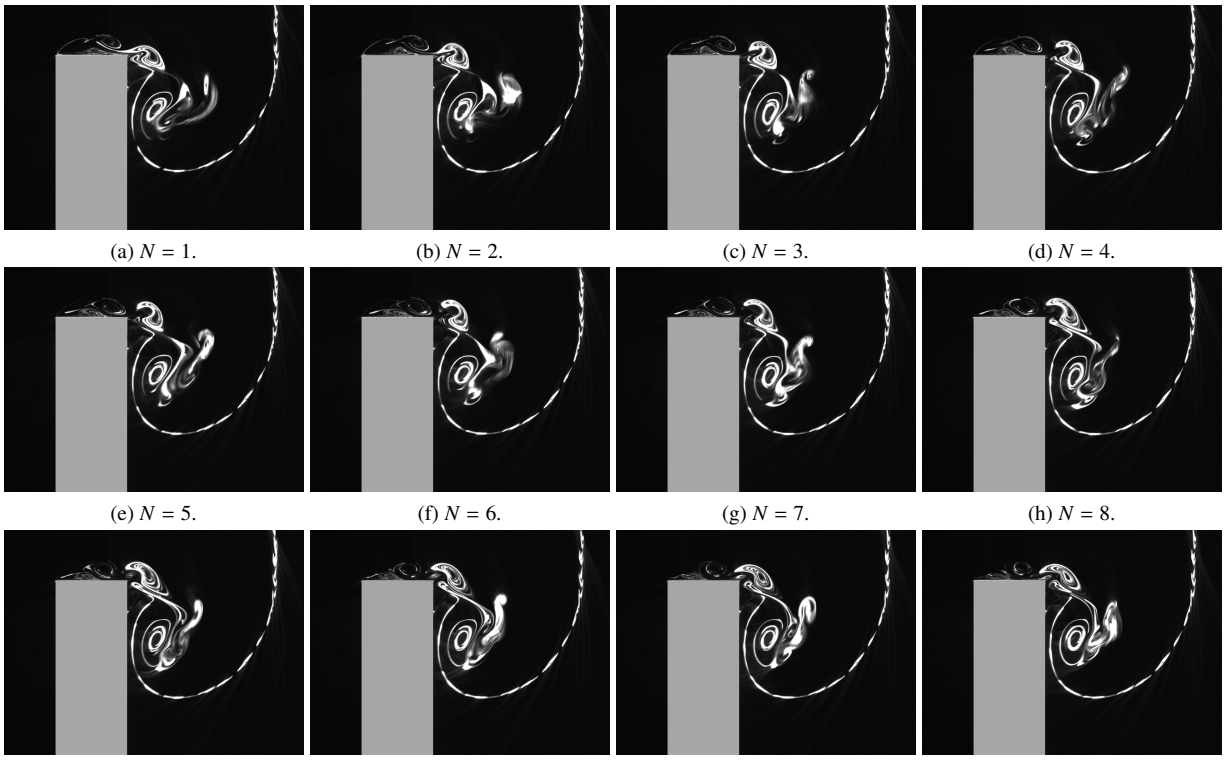

(a) $N = 1$. (b) $N = 2$. (c) $N = 3$. (d) $N = 4$.

(e) $N = 5$. (f) $N = 6$. (g) $N = 7$. (h) $N = 8$.

(i) $N = 9$. (j) $N = 10$. (k) $N = 11$. (l) $N = 12$.

Figure 10: Smoke visualizations snapshots at $f = 30$ Hz, $Re = 3000$, $\alpha = 12^\circ$, $\tilde{x}/c = 0.7$ on squared tip.

[5] J. Katz, J. B. Galdo, Effect of roughness on rollup of tip vortices on a rectangular hydrofoil, Journal of Aircraft 26 (3) (1989) 247–253.

[6] T. B. Francis, D. A. Kennedy, Formation of a trailing vortex, Journal of Aircraft 16 (3) (1979) 148–154.

[7] S. C. C. Bailey, S. Tavoularis, B. H. K. Lee, Effects of freestream turbulence on wing-tip vortex formation and near field, Journal of Aircraf 43 (2006) 1282–1291.

[8] D. Birch, T. Lee, F. Mokhatarian, F. Kafyeke, Rollup and near-field behavior of a tip vortex, Journal of Aircraft 40 (3) (2003) 603–607.

[9] C. Karakus, H. Akilli, B. Sahin, Formation, structure, and development of the near-field wing tip vortices, Proceedings of the Institution of Mechanical Engineers, Part G: Journal of Aerospace Engineering 222 (2008) 13–22.

[10] L. Zuhal, M. Gharib, Near field dynamics of wing tip vortices, in: 31st AIAA Fluid Dynamics Conference & Exhibit, AIAA, Anaheim, CA, 2001.

[11] L. Jacquin, D. Fabre, P. Geffroy, The properties of a transport aircraft wake in the extended near field: an experimental study, in: 39th AIAA Aeropace Sciences Meeting & Exhibit, AIAA, Reno, NV, 2001.

[12] S. C. C. Bailey, S. Tavoularis, Measurements of the velocity field of a wing-tip vortex, wandering in grid turbulence, Journal of Fluid Mechanics 601 (2008) 281–315.

[13] W. J. Devenport, M. C. Rife, S. I. Lipias, G. J. Follin, The structure and development of a wing-tip vortex, Journal of Fluid Mechanics 312 (1996) 67–106.

[14] M. Ramasamy, B. Johnson, T. Huismann, J. G. Leishman, Digital particle image velocimetry measurements of tip vortex characteristic using an improved aperiodicity correction, Journal of the American Helicopter Society 54 (012004).

[15] P. R. Spalart, Airplane trailing vortices, Annual Review of Fluid Mechanics 30 (1998) 107–138.

[16] P. G. Saffman, D. W. Moore, Axial flow in laminar trailing vortices, Proceedings of the Royal Society A (333) (1973) 491–508.

[17] E. R. Hoffmann, P. N. Joubert, Turbulent line vortices, Journal of Fluid Mechanics 16 (1963) 395–411.

[18] W. R. C. Phillips, The turbulent trailing vortex during roll-up, Journal of Fluid Mechanics 105 (1981) 451–467.

[19] A. J. Cotel, R. E. Breidenthal, Turbulence inside a vortex, Physics of Fluids 11 (10) (1999) 3026–3029.

[20] J. S. Chow, G. G. Zilliac, P. Bradshaw, Mean and turbulence measurements in the near field of a wingtip vortex, AIAA Journal 35 (10) (1997) 1561–1567.

[21] W. Zang, K. Prasad, Performance evaluation of a Scheimpflug stereocamera for particle image velocimetry, Applied Optics 36 (33) (1997) 8738–8744.

[22] N. J. Lawson, J. Wu, Three-dimensional particle image velocimetry: error analysis of stereoscopic techniques, Measurements Science and Technology 8 (1997) 894–900.

[23] R. D. Keane, R. J. Adrian, Theory of cross-correlation analysis of PIV images, Applied Scientific Research 49 (1992) 191–215.

[24] M. Giuni, E. Benard, R. B. Green, Investigation of a trailing vortex near field by stereoscopic particle image velocimetry, in: 49th AIAA Aerospace Sciences Meeting, American Institute of Aeronautics and Astronautics, Orlando, FL, 2011.

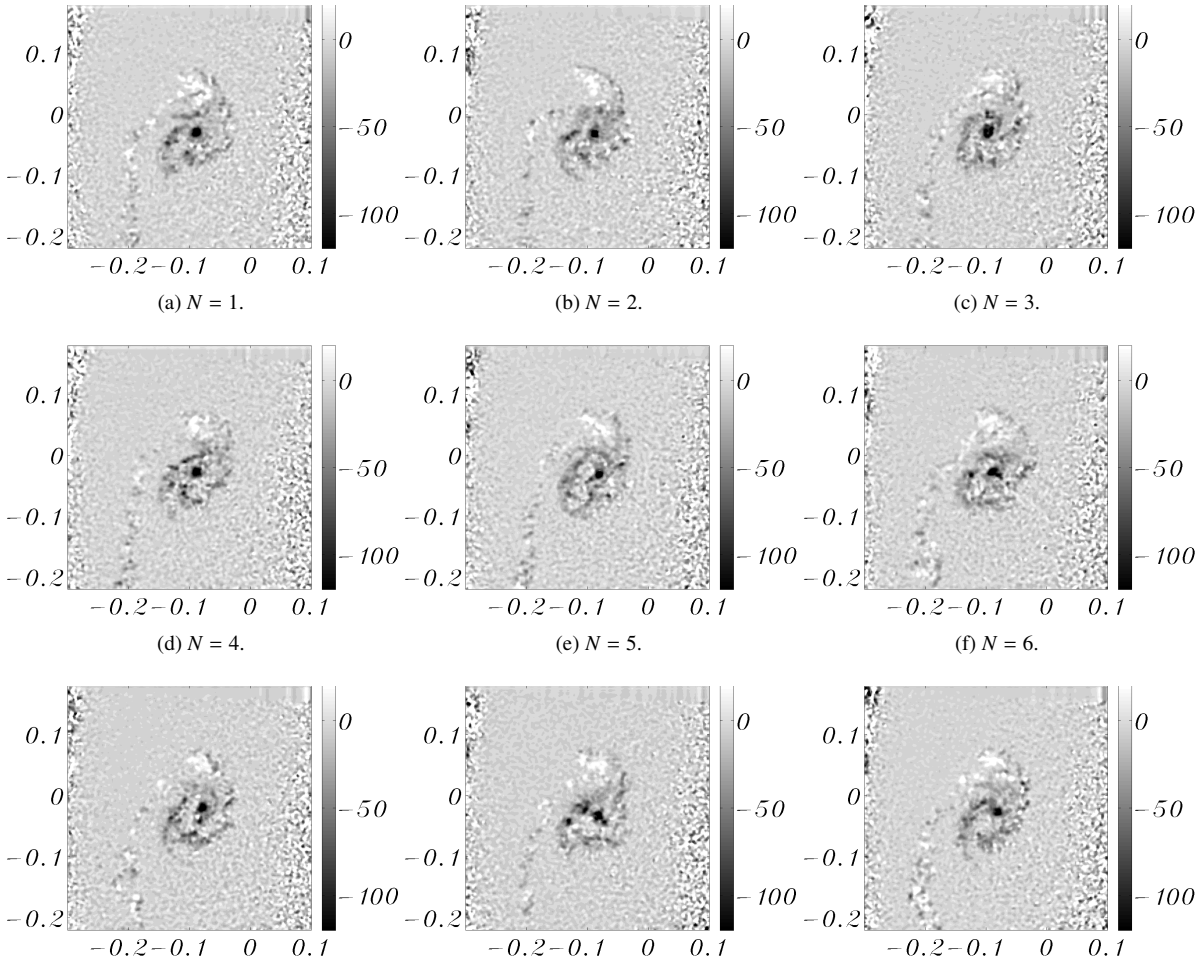

(a) $N = 1$. (b) $N = 2$. (c) $N = 3$.

(d) $N = 4$. (e) $N = 5$. (f) $N = 6$.

(g) $N = 7$. (h) $N = 8$. (i) $N = 9$.

Figure 11: Vorticity snapshots at $f = 2$ Hz, $Re = 760,000$, $\alpha = 12°$, $x/c = 0.25$ on squared tip.

[25] DaVis, DaVis 7.2 Software - Product Manual, LaVision GmbH, Germany, 2007.

[26] R. J. Adrian, Particle-imaging technique for experimental fluid mechanics, Annual Review of Fluid Mechanics 23 (1991) 261–304.

[27] A. K. Prasad, R. J. Adrian, C. C. Landreth, P. W. Offutt, Effect of resoluation on the speed and accuracy of particle image velocimetry interrogation, Experiments in Fluids 13 (1992) 105–116.

[28] M. Raffel, C. Willert, S. Wereley, J. Kompenhans, Particle image velocimetry: a practical guide, Springer, 2nd edn., 2007.

[29] K. Duraisamy, Studies in tip vortex formation, evolution and control, Ph.D. thesis, University of Maryland, College Park, 2005.

[30] T. B. Francis, J. Katz, Observations on the development of a tip vortex on a rectangular hydrofoil, Journal of Fluids Engineering 110 (1988) 208–215.

[31] J. Jeong, F. Hussain, On the identification of a vortex, Journal of Fluid Mechanics 285 (1995) 69–94.

[32] R. Cucitore, M. Quadrio, A. Baron, On the effectiveness and limitations of local criteria for the identification of a vortex, European Journal of Mechanics - B/Fluids 18 (2) (1999) 261–282.

[33] R. J. Adrian, K. T. Christensen, Z. C. Liu, Analysis and interpretation of instantaneous turbulent velocity fields, Experiments in Fluids 29 (2000) 275–290.

[34] G. Haller, An objective definition of a vortex, Journal of Fluid Mechanics 525 (2005) 1–26.

[35] M. Giuni, E. Benard, Analytical/experimental comparison of the axial velocity in trailing vortices, in: 49th AIAA Aerospace Sciences Meeting, American Institute of Aeronautics and Astronautics, Orlando, FL, 2011.

[36] T. Lee, J. Pereira, Nature of wakelike and jetlike axial tip vortex flows, Journal of Aircraft 47 (6) (2010) 1946–1954.

[37] M. Giuni, E. Benard, R. B. Green, Near field core structure of wing tip vortices, in: Experimental Fluid Mechanics 2010, EFM, Liberec, Czech Republic, 2010.

[38] L. Jiang, J. Cai, C. Liu, Large Eddy Simulation of wing tip vortex in the near field, Tech. Rep. 13, The University of Texas, Arlington, 2007.